2014 IEEE International Conference on Robotics & Automation (ICRA)
Hong Kong Convention and Exhibition Center
May 31 - June 7, 2014. Hong Kong, China

# Simultaneous Control for End-Point Motion and Vibration Suppression of a Space Robot Based on Simple Dynamic Model*

Daichi Hirano[1], Yusuke Fujii[1], Satoko Abiko[2], Roberto Lampariello[3], Kenji Nagaoka[1] and Kazuya Yoshida[1]

***Abstract*— This paper addresses a dynamic model and a control method of a space robot with a rigid manipulator and a flexible appendage. The control method has been developed for performing multiple tasks: end-point motion control and vibration suppression control of a flexible appendage. A simple dynamic model that considers coupling between the manipulator and the flexible appendage is proposed for the control method. The tasks are performed simultaneously on the basis of their order of priorities using a redundant manipulator. Additionally, because vibration suppression requires feedback of the state of the flexible appendage, a state estimator of the appendage using a force/torque sensor is developed. Finally, the proposed model, control method, and state estimator were verified experimentally using an air-floating system.**

## I. INTRODUCTION

Demand of on-orbit service robot has increased in recent decades [1]. Space robots for space debris removal or space structure construction are equipped with manipulators and flexible appendages such as solar panels and antennas, as shown in Fig. 1. Manipulators are used for executing required tasks; however manipulator motion and contact with the space debris or space structures induce vibrations in the flexible appendage due to dynamic coupling effects of the system. These vibrations decrease the operation accuracy and increase the risk of mission failure. An appropriate control method considering such effects is required for performing a required task securely.

Control theory for a free-flying robot with a rigid manipulator was discussed on the basis of an articulated body system in several literatures [2][3]. However, research on the control of a space robot that considers the coupling between rigid manipulators and flexible appendages is limited. Zarafshan and Moosavian studied the dynamics and control of such a system in [4]. However, their study ignored dynamic coupling, which can cause closed-loop instability [5].

Nenchev et al. proposed a reactionless control method in [6], which realizes manipulator motion without exciting base motion by using the null-space of a redundant manipulator.

*This research was partially supported by a Grant-in-Aid for JSPS Fellows (23-6651).

[1]D. Hirano, Y. Fujii, K. Nagaoka and K. Yoshida are with Department of Aerospace Engineering, Graduate School of Engineering, Tohoku University, 6-6-1 Aramaki, Aoba-ku, Sendai, 980-8579, Japan {hirano, y-fujii, nagaoka, yoshida} at astro.mech.tohoku.ac.jp

[2]S. Abiko is with Department of Mechanical Systems and Design, Graduate School of Engineering, Tohoku University, 6-6-1 Aramaki, Aoba-ku, Sendai, 980-8579, Japan abiko at space.mech.tohoku.ac.jp

[3]R. Lampariello is with the Institute of Robotics and Mechatronics, German Aerospace Center (DLR), Germany Roberto.Lampariello at dlr.de

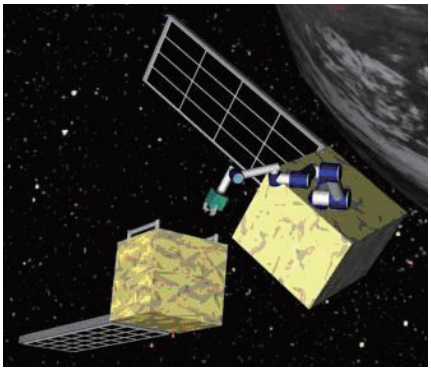

Fig. 1. Image of on-orbit servicing robot

However, this method is inadequate for tasks requiring arbitrary manipulator motion over large areas because manipulator motion is severely restricted by null-space limitations.

The modeling of flexible appendages is a key issue in vibration suppression control. For analyzing flexible appendage behavior, the assumed mode method and the finite element method are commonly used [7][8]. In general, however, the assumed mode method requires several sensors such as piezoelectric elements on the appendage or a visual monitoring system for measuring flexible appendage state, which increase system and operational complexity. In addition, the finite element method is impractical for online feedback control because its calculation cost is enormously high. In our research, therefore, we employ the virtual joint model proposed by Yoshikawa [9], which approximates flexible manipulators as virtual rigid links and passive spring joints. This model expresses a complex flexible appendage as a simple articulated body with dominant dynamic characteristics. Using this method, a free-flying robot with flexible appendages can be modeled as a reduced articulated body system. This reduced model makes it possible to calculate robot dynamics in real time using limited computational resources.

In a previous research, we developed a simple dynamic model of a space robot with a rigid manipulator and a flexible appendage using the virtual joint model for suppressing vibrations of the flexible appendage [10]. In addition, we designed a state estimator for the flexible appendage to achieve control using a force/torque sensor attached between the robot base and the appendage. However, the control method in [10] did not consider end-point motion, while vibration suppression was implemented successfully. In this paper, the simultaneous control method, which implements the end-point motion control and the vibration suppression

control of the flexible appendage, is derived on the basis of a proposed simple model. In addition, an experiment using an air-floating system is conducted for verifying the performance of the proposed dynamic model, control method, and state estimator.

## II. DYNAMIC MODEL

This section briefly reviews dynamic models for a flexible appendage and a robot which were derived in our previous research [10].

### A. Dynamic Model of Flexible Appendage

A cantilever with a tip mass was considered as a flexible appendage, as shown in Fig. 2 (a). We approximated the cantilever as a virtual joint model with one rigid link and one passive joint, as shown in Fig. 2 (b). Reaction torque $\tau_f$ is applied to the rigid link around the virtual joint. We assumed that the reaction torque is linear with respect to the virtual joint angle, and identified the joint stiffness $K_f$ by comparing the eigenfrequencies of the above mentioned models.

The cantilever was assumed to be a Euler-Bernoulli beam. From the Rayleigh law, the first eigenfrequency is given as follows:

$$f_b = \frac{1}{2\pi}\sqrt{\frac{3EI}{l_f^3(m_t + \frac{33}{140}m_s)}} \tag{1}$$

where $E$, $I$, $l_f$, $m_s$, and $m_t$ denote Young's modulus, second moment of the area, length, mass of beam, and mass of the tip, respectively.

In contrast, the eigenfrequency of the virtual joint model is given as follows:

$$f_j = \frac{1}{2\pi}\sqrt{\frac{K_f}{I_f}} \tag{2}$$

where $I_f$ stands for the link's moment of inertia.

From the condition that the above eigenfrequencies are equal, joint stiffness can be calculated as follows.

$$K_f = \frac{3EI}{l_f^3(m_t + \frac{33}{140}m_s)}I_f \tag{3}$$

### B. Dynamic Model of Free-Flying Robot

A simple dynamic model is introduced here with a manipulator and flexible appendage, which is approximated with the virtual joint model. As an example, Fig. 3 shows a dynamic model with a three-joint manipulator and a one-joint flexible appendage. We assumed that the robot is in a micro-gravity environment; therefore, gravity does not apply. Given that no external force and moment are exerted on the end-point and base, the equation of motion of this free-flying system is as follows [2]:

$$\begin{bmatrix} \boldsymbol{H}_b & \boldsymbol{H}_{bm} & \boldsymbol{H}_{bf} \\ \boldsymbol{H}_{bm}^T & \boldsymbol{H}_m & \boldsymbol{H}_{mf} \\ \boldsymbol{H}_{bf}^T & \boldsymbol{H}_{mf}^T & \boldsymbol{H}_f \end{bmatrix} \begin{bmatrix} \ddot{\boldsymbol{x}}_b \\ \ddot{\boldsymbol{\phi}}_m \\ \ddot{\boldsymbol{\phi}}_f \end{bmatrix} + \begin{bmatrix} \boldsymbol{c}_b \\ \boldsymbol{c}_m \\ \boldsymbol{c}_f \end{bmatrix} = \begin{bmatrix} \boldsymbol{0} \\ \boldsymbol{\tau}_m \\ \boldsymbol{\tau}_f \end{bmatrix} \tag{4}$$

where the symbols are defined as follows.

$\boldsymbol{H}_b$ : Inertia matrix of base

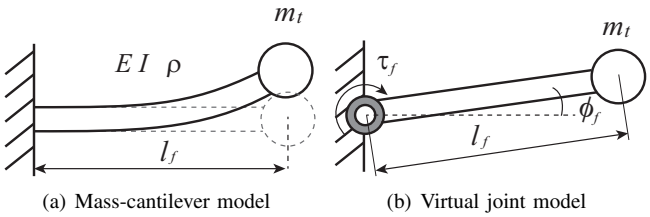


(a) Mass-cantilever model (b) Virtual joint model

Fig. 2. Flexible appendage model

$\boldsymbol{H}_m$ : Inertia matrix of manipulator
$\boldsymbol{H}_f$ : Inertia matrix of flexible appendage
$\boldsymbol{H}_{bm}$ : Inertia matrix of coupling between base and manipulator
$\boldsymbol{H}_{bf}$ : Inertia matrix of coupling between base and flexible appendage
$\boldsymbol{H}_{mf}$ : Inertia matrix of coupling between manipulator and flexible appendage
$\boldsymbol{x}_b$ : Base position and orientation vector
$\boldsymbol{\phi}_m$ : Manipulator angle vector
$\boldsymbol{\phi}_f$ : Flexible appendage angle vector
$\boldsymbol{c}_b$ : Nonlinear velocity-dependent term of base
$\boldsymbol{c}_m$ : Nonlinear velocity-dependent term of manipulator
$\boldsymbol{c}_f$ : Nonlinear velocity-dependent term of flexible appendage
$\boldsymbol{\tau}_m$ : Vector of torque on manipulator joints
$\boldsymbol{\tau}_f$ : Vector of torque on flexible appendage joints.

The torque of the flexible appendage is given by the following linearized form:

$$\boldsymbol{\tau}_f = -\boldsymbol{K}_f\boldsymbol{\phi}_f - \boldsymbol{D}_f\dot{\boldsymbol{\phi}}_f \tag{5}$$

where $\boldsymbol{K}_f$ and $\boldsymbol{D}_f$ denote the matrices of the flexible appendage's stiffness and damping, respectively.

By eliminating the base acceleration term $\ddot{\boldsymbol{x}}_b$ from the middle and lower parts of (4) using the upper part of (4), the equation of motion can be rewritten in the following joint coordinate form:

$$\hat{\boldsymbol{H}}\begin{bmatrix} \ddot{\boldsymbol{\phi}}_m \\ \ddot{\boldsymbol{\phi}}_f \end{bmatrix} + \hat{\boldsymbol{c}} = \begin{bmatrix} \boldsymbol{\tau}_m \\ \boldsymbol{\tau}_f \end{bmatrix} \tag{6}$$

where

$$\hat{\boldsymbol{H}} = \begin{bmatrix} \boldsymbol{H}_m & \boldsymbol{H}_{mf} \\ \boldsymbol{H}_{mf}^T & \boldsymbol{H}_f \end{bmatrix} - \boldsymbol{H}_{bc}^T\boldsymbol{H}_b^{-1}\boldsymbol{H}_{bc} \tag{7}$$

$$\hat{\boldsymbol{c}} = \begin{bmatrix} \boldsymbol{c}_m \\ \boldsymbol{c}_f \end{bmatrix} - \boldsymbol{H}_{bc}^T\boldsymbol{H}_b^{-1}\boldsymbol{c}_b \tag{8}$$

$$\boldsymbol{H}_{bc} = [\boldsymbol{H}_{bm}\;\; \boldsymbol{H}_{bf}]. \tag{9}$$

The matrix $\hat{\boldsymbol{H}}$ is referred to as the generalized inertia matrix.

## III. CONTROL METHOD

### A. End-Point Control

The end-point velocity of a free-flying robot can be expressed as follows:

$$\dot{\boldsymbol{x}}_e = \boldsymbol{J}_g\dot{\boldsymbol{\phi}} \tag{10}$$

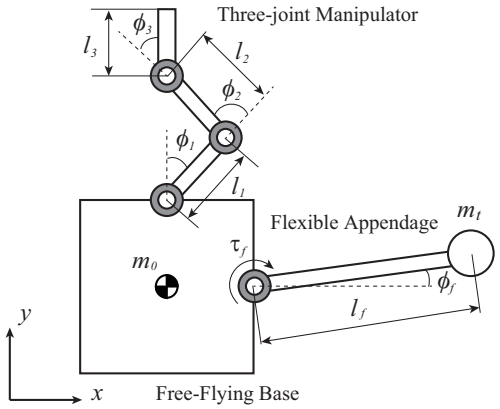


Fig. 3. Dynamic model of free-flying robot with three-joint manipulator and flexible appendage

where $\dot{\boldsymbol{x}}_e$ denotes the vector of end-point velocity, $\boldsymbol{J}_g$ denotes the generalized Jacobian matrix, and $\boldsymbol{\phi}$ stands for an angle vector of the manipulator and the flexible appendage ($\boldsymbol{\phi} = [\boldsymbol{\phi}_m^T \, \boldsymbol{\phi}_f^T]^T$). The right-hand side of (10) can be divided into manipulator and flexible appendage terms as follows.

$$\dot{\boldsymbol{x}}_e = \boldsymbol{J}_{gm}\dot{\boldsymbol{\phi}}_m + \boldsymbol{J}_{gf}\dot{\boldsymbol{\phi}}_f \tag{11}$$

where $\boldsymbol{J}_{gm}$ and $\boldsymbol{J}_{gf}$ are generalized Jacobian components of the manipulator and the flexible appendage, respectively. In a redundant robotic system with respect to the operational space task of end-point, the inverse solution of (11) can be written as follows:

$$\dot{\boldsymbol{\phi}}_m = \boldsymbol{J}_{gm}^{+}(\dot{\boldsymbol{x}}_e - \boldsymbol{J}_{gf}\dot{\boldsymbol{\phi}}_f) + (\boldsymbol{I} - \boldsymbol{J}_{gm}^{+}\boldsymbol{J}_{gm})\boldsymbol{\zeta} \tag{12}$$

where the superscript "+" denotes the pseudo inverse, $\boldsymbol{I}$ denotes the identity matrix, and $\boldsymbol{\zeta}$ denotes an arbitrary vector. The second term in the right-hand side of (12) is called null space and can be utilized for an additional task using the manipulator redundancy.

### B. Vibration Suppression Control

The basic law of vibration suppression was introduced in [11]. Using (5), the lower part of (6) can be expressed with the components of $\hat{\boldsymbol{H}}$ and $\hat{\boldsymbol{c}}$ as follows:

$$\hat{\boldsymbol{H}}_{fm}\ddot{\boldsymbol{\phi}}_m + \hat{\boldsymbol{H}}_f\ddot{\boldsymbol{\phi}}_f + \hat{\boldsymbol{c}}_f + \boldsymbol{D}_f\dot{\boldsymbol{\phi}}_f + \boldsymbol{K}_f\boldsymbol{\phi}_f = \boldsymbol{0} \tag{13}$$

where $\hat{\boldsymbol{H}}_f$ and $\hat{\boldsymbol{H}}_{fm}$ are components of the generalized inertia matrix for the flexible appendage and the coupling term between the manipulator and flexible appendage, respectively, and $\hat{\boldsymbol{c}}_f$ is a component of $\hat{\boldsymbol{c}}$ for the flexible appendage. By choosing manipulator acceleration that satisfies:

$$\hat{\boldsymbol{H}}_{fm}\ddot{\boldsymbol{\phi}}_m = \boldsymbol{D}_c\dot{\boldsymbol{\phi}}_f - \hat{\boldsymbol{c}}_f \tag{14}$$

where $\boldsymbol{D}_c$ denotes a control gain matrix, flexible appendage vibration is suppressed according to the following equation of motion of a damping system.

$$\hat{\boldsymbol{H}}_f\ddot{\boldsymbol{\phi}}_f + (\boldsymbol{D}_c + \boldsymbol{D}_f)\dot{\boldsymbol{\phi}}_f + \boldsymbol{K}_f\boldsymbol{\phi}_f = \boldsymbol{0} \tag{15}$$

Note that the control gain $\boldsymbol{D}_c$ changes the system damping ratio. By adding a damping term to the inverse solution of (14), we obtain the manipulator's desired angular acceleration as follows:

$$\ddot{\boldsymbol{\phi}}_m^d = \hat{\boldsymbol{H}}_{fm}^{+}(\boldsymbol{D}_c\dot{\boldsymbol{\phi}}_f - \hat{\boldsymbol{c}}_f) - \boldsymbol{D}_q\dot{\boldsymbol{\phi}}_m \tag{16}$$

where $\boldsymbol{D}_q$ stands for a manipulator joint damping matrix. By integrating the desired angular acceleration in (16) and adding it to the current angular velocity, the manipulator's desired angular velocity for vibration suppression can be obtained as follows:

$$\dot{\boldsymbol{\phi}}_m^d = \dot{\boldsymbol{\phi}}_m + \int_t^{t+\Delta t}\{\hat{\boldsymbol{H}}_{fm}^{+}(\boldsymbol{D}_c\dot{\boldsymbol{\phi}}_f - \hat{\boldsymbol{c}}_f) - \boldsymbol{D}_q\dot{\boldsymbol{\phi}}_m\}dt \tag{17}$$

where $t$ and $\Delta t$ denote the experimental time and the control loop time, respectively.

### C. Simultaneous Control

Simultaneous control methods using redundant manipulators can be classified in two approaches: task-space augmentation and task-priority resolution. The task-space augmentation approach uses a square matrix built from the constraints on a primary task and an additional task. Such a square matrix is called the extended Jacobian or the augmented Jacobian and is used for resolving a proper manipulator joint motion via its inverse matrix. However, this approach does not consider the priority order of these tasks, and therefore, the solution becomes unfeasible for both tasks around an algorithmic singularity, which is a configuration where the tasks are in conflict with each other. In contrast, the task-priority resolution approach provides a proper solution based on the priority order of the given tasks [12]. Under this approach, the lower-priority task is executed using a null space of the higher-priority task. In addition, using the lower-priority relaxation based on the task-priority resolution in [13], this approach can implement the higher-priority task even around an algorithmic singularity by reducing the null space component for the lower-priority task. In this paper, we derived a control law according to this approach.

In general, end-point motion control is considered as the primary task over vibration suppression control of the flexible appendage because end-point motion errors cause result in severe failure such as an undesired collision with a free-flying object. According this order of priority, the desired manipulator angular velocity for simultaneous control is given from (12) and (17) as follows:

$$\dot{\boldsymbol{\phi}}_m^d = \boldsymbol{J}_{gm}^{+}(\dot{\boldsymbol{x}}_e^d - \boldsymbol{J}_{gf}\dot{\boldsymbol{\phi}}_f) + (\boldsymbol{I} - \boldsymbol{J}_{gm}^{+}\boldsymbol{J}_{gm})\left(\dot{\boldsymbol{\phi}}_m + \int_t^{t+\Delta t}\{\hat{\boldsymbol{H}}_{fm}^{+}(\boldsymbol{D}_c\dot{\boldsymbol{\phi}}_f - \hat{\boldsymbol{c}}_f) - \boldsymbol{D}_q\dot{\boldsymbol{\phi}}_m\}dt\right) \tag{18}$$

where $\dot{\boldsymbol{x}}_e^d$ denotes the desired end-pint velocity. This control law preferentially implements end-point control and performs vibration suppression for flexible appendage using the null space of end-point control. Note that this control law requires feedback of the angle and the angular velocity on the flexible appendage's virtual joint. The state estimator of the flexible appendage for this feedback control is presented in the next section.

### D. Design of Flexible Appendage State Estimator

In case that the flexible appendage is modeled as a single virtual joint, the angular velocity of this virtual joint can be estimated using the force/torque sensor attached between the base and the flexible appendage.

Assuming that the damping term is negligibly small, the virtual joint angle can be expressed as follows using (5):

$$\phi_f = \frac{\tau_f}{K_f} \tag{19}$$

where $\tau_f$ denotes the torque measured by the force/torque sensor. The angular velocity $\dot{\phi}_f$, which is used for feedback control, can be obtained numerically from the differential value of $\phi_f$ provided by (19).

## IV. EXPERIMENT

An experimental study was conducted for validating the proposed control scheme based on the simplified model and estimated feedback value.

### A. Assumptions

The feedback values are obtained from the state estimator described in the above section. The control law given by (18) requires the calculation of $\boldsymbol{J}_{gf}$, $\hat{\boldsymbol{H}}_{fm}$ and $\hat{\boldsymbol{c}}_f$, which are obtained from the inertia matrices $\boldsymbol{H}_b$ and $\boldsymbol{H}_{bc}$. These inertia matrices are functions of the virtual joint angle $\boldsymbol{\phi}_f$. However, the angle $\phi_f$ is difficult to be measured using the force/torque sensor because the force/torque sensor often has offset error, while the angular velocity $\dot{\phi}_f$ is not affected by this offset because it is obtained via differentiation. In this experiment, therefore, approximated inertia matrices that do not depend on the virtual joint angle are used for calculating the control input.

Suppose that the virtual joint angle of the flexible appendage is small and the inertia matrices can be approximated as the values around the equilibrium point, i.e.,

$$\boldsymbol{H}_b(\boldsymbol{\phi}_b, \boldsymbol{\phi}_m, \phi_f) \simeq \boldsymbol{H}_b(\boldsymbol{\phi}_b, \boldsymbol{\phi}_m, 0) \tag{20}$$

$$\boldsymbol{H}_{bc}(\boldsymbol{\phi}_b, \boldsymbol{\phi}_m, \phi_f) \simeq \boldsymbol{H}_{bc}(\boldsymbol{\phi}_b, \boldsymbol{\phi}_m, 0) \tag{21}$$

where $\boldsymbol{\phi}_b$ denotes the base attitude vector. From the above approximations, the inertia matrices turn into functions that do not depend on the virtual joint angle. These approximated inertia matrices were tested in our previous research, and the control ability using them was experimentally confirmed in [10].

### B. Experimental Setup

We developed an air-floating system that can emulate planar motion under a micro-gravity environment using an air bearing, as shown in Fig. 4. This system uses pressurized air to float up a robot on a flat plane for realizing frictionless motion between the robot and the plane. The robot is equipped with a three-joint manipulator and a flexible appendage. The robot parameters are listed in Table I. The symbols in this list are the same as those in Fig. 3. Furthermore, this robot has a gyroscope on its base, which measures its angle and angular velocity of rotation. The manipulator encoders provide each joint angles and angular velocities. The flexible appendage is a cantilever with a tip mass and is attached to the robot base through a force/torque sensor that measures the appendage's angular velocity (see Fig. 4). The values measured using the gyroscope, manipulator encoders, and force/torque sensor are used for feedback control. The dynamic calculation and input-output data transfer for the control are performed by an on-board computer.

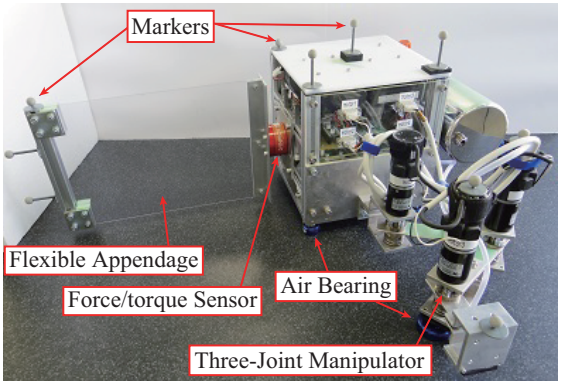


Fig. 4. Air-floating system

TABLE I
MODEL PARAMETER VALUES

| | | |
|---|---|---|
| $l_1, l_2$ | 0.120 | [m] |
| $l_3$ | 0.067 | [m] |
| $l_f$ | 0.300 | [m] |
| $m_0$ | 8.170 | [kg] |
| $m_1$ | 0.555 | [kg] |
| $m_2$ | 0.621 | [kg] |
| $m_3$ | 0.267 | [kg] |
| $m_t$ | 0.320 | [kg] |
| $K_f$ | 0.556 | [Nm/rad] |

The motions of the robot and the flexible appendage were measured using external motion capture cameras that track markers on the robot and the flexible appendage, as shown in Fig. 5.

### C. Experimental Conditions

Using the developed robot with the flexible appendage, we conducted two different experiments: (i) end-point control based on a fully-rigid model and (ii) simultaneous control based on the proposed dynamic model. In (i), appendage flexibility is ignored, and the appendage is considered as a rigid body attached to the base. In contrast, in (ii), a flexible appendage is modeled using the virtual joint model, and the control scheme simultaneously implements end-point control and vibration suppression control for the appendage. In both cases, only the end-point position ($x_e$ and $y_e$) is considered for end-point control, and its orientation is not controlled. In (ii), the end-point control is implemented using two degrees of freedom of the three-joint manipulator, and the vibration suppression control is performed using one degree of freedom.

In both the experiments, the initial state was stable and the initial joint angles were $\boldsymbol{\phi}_m = [\ 90 \quad -45 \quad -45\ ]^T$[deg]. In

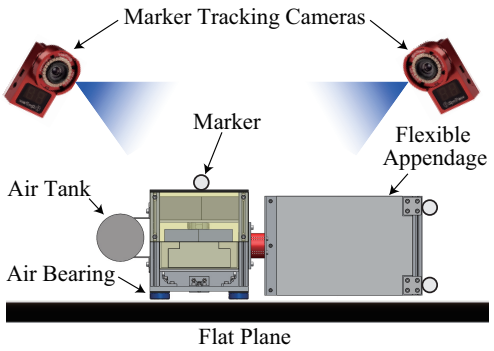


Fig. 5. Overview of experimental setup

addition, the desired end-point velocity for ensuring smooth motion was given as follows:

$$\dot{\boldsymbol{x}}_e^d = \begin{cases} [\dot{x}_e^d \quad 0 \quad 0]^T \quad [\text{deg/s}] \quad (0 \le t < t_f) \\ [0 \quad 0 \quad 0]^T \quad [\text{deg/s}] \quad (t_f \le t) \end{cases} \tag{22}$$

where

$$\dot{x}_e^d = 3at^2 + 4bt^3 + 5ct^4 \tag{23}$$

$$a = \frac{10x_f}{t_f^3}, \quad b = -\frac{15x_f}{t_f^4}, \quad c = \frac{6x_f}{t_f^5} \tag{24}$$

and $t_f$ denotes the time during the end-point moves, and $x_f$ denotes the the end-point motion distance in $t_f$. In these experiments, $t_f$ and $x_f$ were set as $t_f = 3$ [s] and $x_f = 0.2$ [m]. Fig. 6 shows the motion sequence of the robot. The distance between the initial and final end-point positions, i.e., the length of the desired path is 0.2 m. During the first 3 s, the end-point approaches the goal point, and appendage vibrations are induced. After 3 s, the end-point remains at the goal point with and without suppressing the appendage vibrations.

In (i), because the fully-rigid model does not have the virtual joint of the flexible appendage, the manipulator control input is given as follows.

$$\dot{\boldsymbol{\phi}}_m^d = \boldsymbol{J}_g^+ \dot{\boldsymbol{x}}_e^d \tag{25}$$

In contrast, in (ii), the manipulator control input is given as an angular velocity in (18). The control gains were set to $D_c = 5.0$ and $D_q = 1.0$. The feedback value $\dot{\phi}_f$ was obtained using the state estimator. A block diagram of the control scheme is shown in Fig. 7. In this experiment, the control loop was set to 2 ms.

### D. Results and Discussion

Fig. 8 shows snapshots of the robot motion sequence in experiments (i) and (ii). Fig. 9 shows detailed graphs of the experimental results. In this figure, the results of experiment (i) are indicated by dotted lines and those of experiment (ii) are shown by solid lines.

Fig. 9 (a) shows the result of manipulator joint angles. In (i), manipulator motion was stopped at $t = 3$ [s] because the desired end-point velocity decreased to 0 m/s after this moment. In contrast, in (ii), the manipulator continued moving even after $t = 3$ [s] for suppressing vibrations

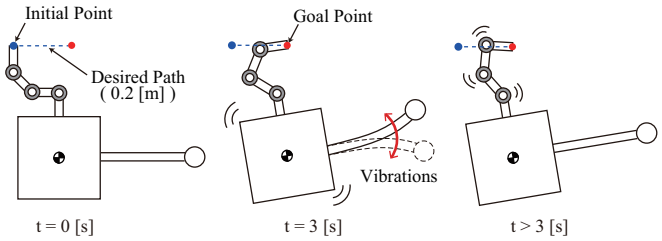


Fig. 6. Robot motion sequence

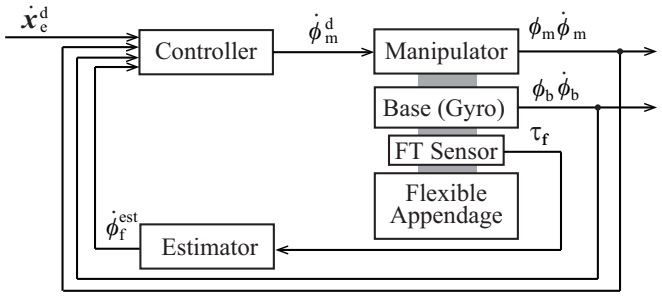


Fig. 7. Control block diagram

of the flexible appendage, while the end-point maintained it's position. Such manipulator motions are confirmed in Fig. 8 as well. In Fig. 9 (b), the tip deflections of the flexible appendage are compared. The vibration of the flexible appendage was suppressed via the proposed simultaneous control. However, small-amplitude vibrations were not suppressed, while the dominant large-amplitude vibrations were successfully suppressed. This is ascribed to limitations of the manipulator actuator and the sensor. Motion with a small angular velocity is difficult to realize because of hardware limitations. In addition, the small deflections can not be measured precisely owing to electrical noise. Although the noise can be practically reduced using a low-pass filter, noise filtering causes time delay in the control system. Thus, in the experiments, we experimentally regulated the filtering level based on trade-off between the measurement accuracy and the controlled response. Fig. 9 (c) shows the responses of the end-point velocities. In this figure, the desired end-point velocities on the $x$ and $y$ axes are indicated by a green line and a black line, respectively. The errors between the actual velocity and the desired velocity in the experiment (i) during the first 3 s were larger than those in the experiment (ii). In addition, even after the end-point motion input became 0 m/s at $t = 3$ [s], oscillatory errors were observed in (i). These errors are attributed to a loss of a consideration for the appendage flexibility in the control model. In contrast, in (ii) which considers the appendage flexibility, the end-point velocity was sufficiently close to the desired velocity even in periods where the flexible appendage's vibrations were not suppressed. This result indicated that end-point control based on the proposed model can reduce its error. Fig. 9 (d) shows the time history of the angular velocities of the flexible appendage's virtual joint. The estimated angular velocity of the virtual joint in (ii) is indicated by a red line in this figure. Although the estimated value oscillates owing

to force/sensor noise, it was able to estimate the angular velocity, and therefore, the vibration suppression control was realized successfully. Fig. 9 (e) shows the end-point position responses. The desired paths, which are calculated from the desired velocity in (22) and the initial position, are indicated by a green line and a black line. In addition, an enlarged figure showing the end-point position on the $x$ axis is inserted. In this figure, the end-point position in (i) had larger errors in comparison with that in (ii), and it oscillated. These errors in (i) are ascribed to a loss of a consideration for the appendage flexibility. Figs. 9 (b) and (e) show that the simultaneous control implemented the end-point control with suppressing appendage's vibrations. Although vibrations were induced in the appendage because the vibration suppression's priority was assigned secondly, the vibration suppression was performed without disturbing the end-point control. This result indicated that the proposed simultaneous control was successfully implemented according to the assigned order of tasks' priorities. Fig. 9 (f) shows the result of the base attitude. Although drifting of the base owing to low gradient of the air bearing and the ground plane was observed, as a result of the vibration suppression, the base attitude vibrations were also suppressed in the experiment (ii). In contrast, in the experiment (i), the base attitude continued to vibrate because the base was affected by the flexible appendage's vibrations.

The above experimental results proved that the proposed simple model and control method using state estimation for a flexible appendage can adequately and simultaneously control end-point motion and suppress vibrations of a flexible appendage of a free-flying robot.

## V. CONCLUSIONS

This paper presented a simultaneous control method for end-point motion and vibration suppression of a flexible appendage of a space robot. We proposed a simplified dynamic model using a virtual joint model and the state estimator of a flexible appendage using a force/torque sensor. The simultaneous control method using a redundant manipulator was derived on the basis of the proposed model. Practical viability of the control method based on the proposed model and state estimation was verified experimentally using an air-floating system. The experimental results showed that the proposed control scheme is sufficiently able to increase accuracy of end-point motion and suppress vibrations of a flexible appendage.

As future works, a robust observer system and an adaptive control method to guarantee the stability with respect to model errors and sensor noises will be developed. In addition, a three-dimensional verification of the proposed method will be implemented using a hybrid simulator and a real scale robot.

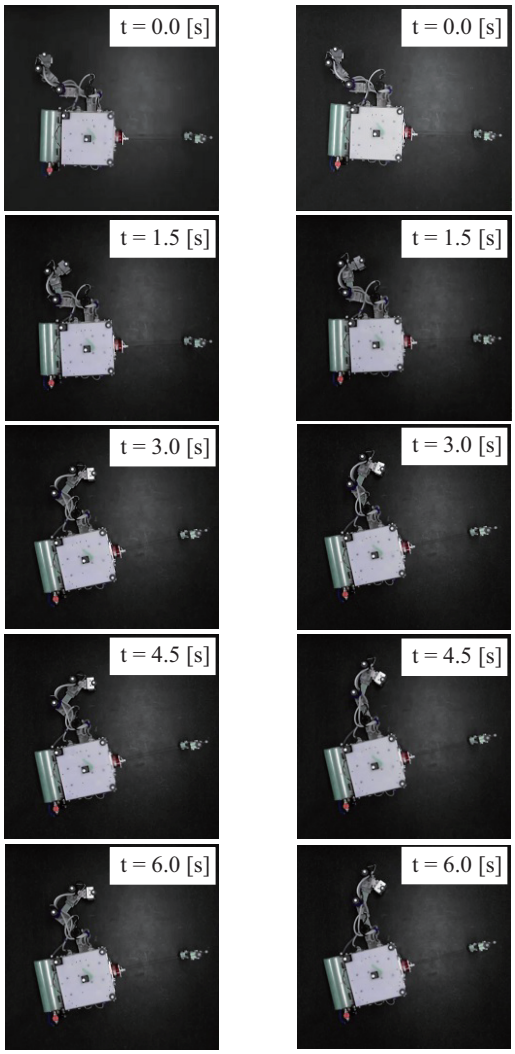


(i) End-Point Velocity Control (ii) Simultaneous Control

Fig. 8. Robot motion sequence

## REFERENCES


[1] G. Hirzinger, et al., DLR's robotics technologies for on-orbit servicing, Advanced Robotics, vol. 18, no. 2, 2004, pp. 139-174.

[2] Y. Xu and T. Kanade, Space robotics: dynamics and control, Kluwer, Dordrecht, 1993, pp. 165-204.

[3] D. N. Nenchev, K. Yoshida, and Y. Umetani, Introduction of redundant arms for manipulation in space, in Proc. 1988 IEEE Int. Workshop on Intelligent Robotics and Systems, Tokyo, Japan, 1988, pp. 679-684.

[4] P. Zarafshan and S. A. A. Moosavian, Manipulation control of a space robot with flexible solar panel, in Proc. 2010 IEEE/ASME Int. Conf. on Advanced Intelligent Mechatronics, Montreal, Canada, 2010, pp. 1099-1104.

[5] J. L. Junkins and Y. Kim, Introduction to dynamics and control of flexible structure, AIAA Inc.,1993, pp. 140.

[6] D. N. Nenchev, et al., Reaction null-space control of flexible structure mounted manipulator systems, IEEE Trans. on Robotics and Automation, vol. 15, no. 6, 1999, pp. 1011-1023.

[7] M. Benosman and G. L. Vey, Control of flexible manipulators: a survey, Robotica, vol. 22, 2004, pp. 533-545.

[8] S. K. Dwivedy and P. Eberhard, Dynamic analysis of flexible manipulators, a literature review, Mechanism and Machine Theory, vol. 41, 2006, pp. 749-777.

[9] T. Yoshikawa and K. Hosoda, Modeling of flexible manipulators using virtual rigid links and passive joints, in Proc. 1991 IEEE/RSJ Int. Conf. on Intelligent Robotics and Systems, Osaka, Japan, 1991, pp. 967-972.

[10] D. Hirano et al., Vibration suppression control of a space robot with flexible appendage based on simple dynamic model, in Proc. 2013 IEEE/RSJ Int. Conf. on Intelligent Robotics and Systems, Tokyo, Japan, 2013, pp. 789-794.

[11] K. Yoshida, D. N. Nenchev, and M. Uchiyama, Vibration suppression and zero reaction maneuvers of flexible space structure mounted

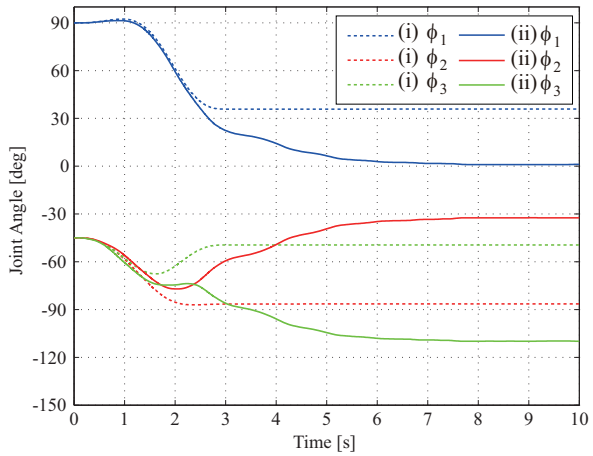


(a) Manipulator joint angles

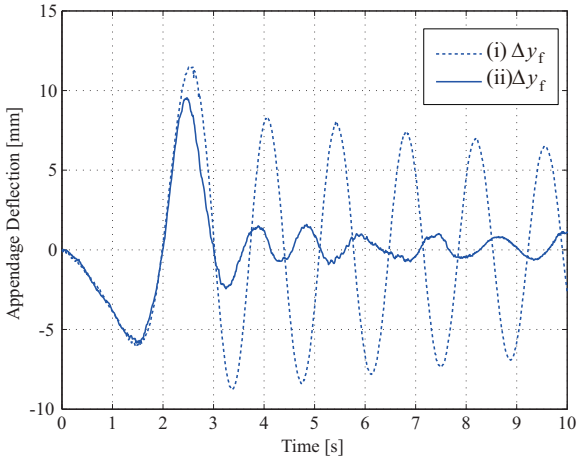


(b) Tip deflections of flexible appendage

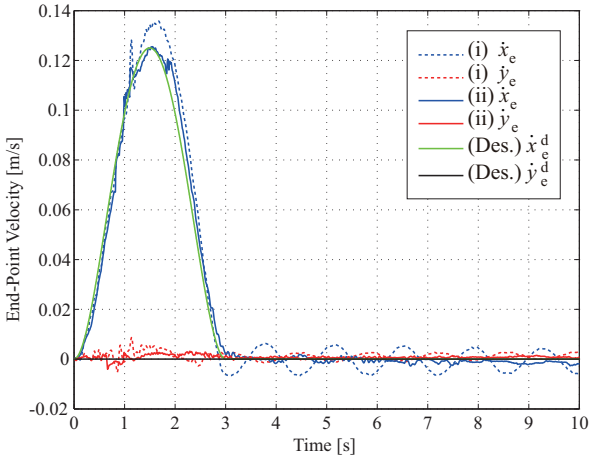


(c) End-point velocity

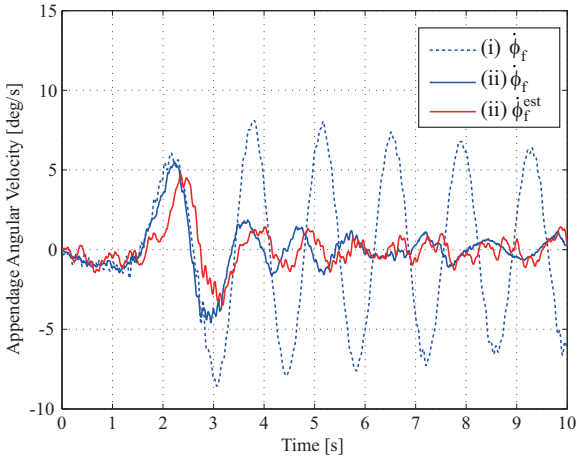


(d) Angular velocities of flexible appendage

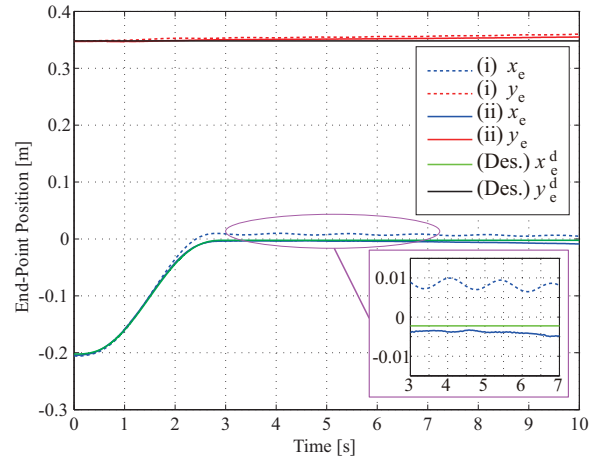


(e) End-point position

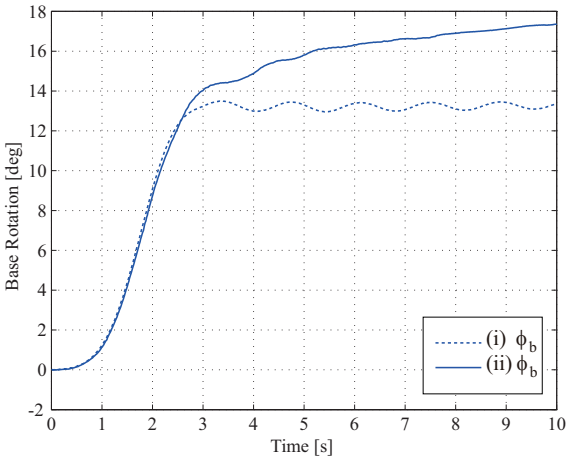


(f) Base attitude rotation

Fig. 9. Experimental results of (i) end-point velocity control based on fully-rigid model and (ii) simultaneous control based on proposed model

manipulators, Smart Materials and Structure, vol. 8, no .6, 1999, pp. 847-856.

[12] Y. Nakamura, H. Hanafusa, and T. Yoshikawa, Task-priority based redundancy control of robot manipulator, The Int. J. of Robotics Research, vol. 6, no. 2, 1987, pp. 3-15.

[13] S. Chiaverini, Singularity-robust task-priority redundancy resolution for real kinematic control of robot manipulators, IEEE Trans. on Robotics and Automation, vol. 13, no. 3, 1997, pp. 398- 410.